

On the temperature dependence of the electrical conductivity in hot quenched lattice QCD

A. Francis^{1,2} and O. Kaczmarek¹

¹Fakultät für Physik, Universität Bielefeld, D-33615 Bielefeld, Germany

²Institut für Kernphysik, Johannes Gutenberg Universität Mainz,
D-55099 Mainz, Germany

June 10, 2018

Abstract

Extending our recent work [1], we report on a calculation of the vector current correlation function for light valence quarks in the deconfined phase of quenched QCD in the temperature range $1.16T_c \lesssim T \lesssim 2.98T_c$. After performing a systematic analysis of the influence of cut-off effects on light quark meson correlators using clover improved Wilson fermions, we discuss resulting constraints on the electrical conductivity in a quark gluon plasma.

1 Introduction

The spectral representation of the correlation functions of the vector current directly relates to the invariant mass spectrum of dileptons and photons. Additionally in the limit of small frequencies it determines a transport coefficient, in the case of the vector correlation function of light quarks, the electrical conductivity.

At temperatures relevant for current heavy ion experiments non-perturbative techniques are mandatory for the determination of these quantities. Perturbative studies of the vector spectral functions [2, 3] and also the inclusion of non-perturbative aspects through the hard thermal loop resummation scheme [4] break down, especially in the low invariant mass region, indicated by an infrared divergent Euclidean correlator [5], leading to an infinite electrical conductivity. However it could be demonstrated that the spectral function at low invariant masses in fact increases linearly resulting in a finite electrical conductivity of the quark gluon plasma [6, 7]. This behavior could also be established by previous work using lattice QCD [8].

In [1] we analyzed the vector correlation function at $T \simeq 1.45T_c$ and performed its extrapolation to the continuum limit based on precise data at various lattice sizes, corresponding to different lattice cutoffs. We then obtained reliable results for the determination of the spectral properties and the extraction of the dilepton rates and transport coefficients. Here we report on a first extension of this work to a wider temperature range and present results on the electrical conductivity in the temperature region $1.16T_c \lesssim T \lesssim 2.98T_c$.

2 Thermal vector correlation and spectral function

The desired information is encoded in the large distance region of temporal Euclidean correlation functions of the vector current at non-zero temperature and fixed spatial momentum,

$$G_{\mu\nu}(\tau, \vec{p}) = \int d^3x \langle J_\mu(\tau, \vec{x}) J_\nu^\dagger(0, \vec{0}) \rangle e^{i\vec{p}\cdot\vec{x}}, \quad \text{where: } J_\mu(\tau, \vec{x}) \equiv \bar{q}(\tau, \vec{x}) \gamma_\mu q(\tau, \vec{x}). \quad (1)$$

Whereby the current-current correlation functions can be represented in terms of an integral over spectral functions, $\rho_{\mu\nu}(\omega, \vec{p}, T)$:

$$G_H(\tau, \vec{p}, T) = \int_0^\infty \frac{d\omega}{2\pi} \rho_H(\omega, \vec{p}, T) \frac{\cosh(\omega(\tau - 1/2T))}{\sinh(\omega/2T)}, \quad H = 00, ii, V, \quad (2)$$

here we denote by ρ_{ii} the sum over the three space-space components of the spectral function and also introduce the vector spectral function $\rho_V \equiv \rho_{00} + \rho_{ii}$.

The time-time component of the vector correlation function, $G_{00}(\tau T)$, is conserved and can be shown to be proportional to the quark number susceptibility, $G_{00}(\tau T) = -\chi_q T$. The vector correlation functions G_{ii} and G_V therefore differ only by a constant,

$$G_V(\tau T) = G_{ii}(\tau T) - \chi_q T. \quad (3)$$

At high temperature and for large energies corrections to the free field behavior can be calculated perturbatively; the vector spectral function can be deduced from the calculation of one loop corrections to the leading order results for the thermal dilepton rate [9]. This yields,

$$\rho_V(\omega) \simeq \frac{3}{2\pi} \left(1 + \frac{\alpha_s}{\pi}\right) \omega^2 \tanh(\omega/4T) \quad , \quad \omega/T \gg 1. \quad (4)$$

In the free field, infinite temperature limit the spatial part of the spectral function contains a δ -function at the origin. Different from the time-time component, where the δ -function is protected by current conservation, this δ -function is smeared out at finite temperature and the low energy part of ρ_{ii} is expected to be described by a Breit-Wigner peak [10, 11, 12],

$$\rho_{ii}^{BW}(\omega) = \chi_q c_{BW} \frac{\omega \Gamma}{\omega^2 + (\Gamma/2)^2}. \quad (5)$$

The limit $\omega \rightarrow 0$ is sensitive to transport properties in the thermal medium and in this case it leads to the electrical conductivity

$$\frac{\sigma}{T} = \frac{C_{em}}{6} \lim_{\omega \rightarrow 0} \frac{\rho_{ii}(\omega)}{\omega T}. \quad (6)$$

The Breit-Wigner form then yields $\sigma(T)/C_{em} = 2\chi_q c_{BW}/(3\Gamma)$. Note here that in the infinite temperature limit the width of the Breit-Wigner peak vanishes, while at the same time $c_{BW} \rightarrow 1$, $\chi_q \rightarrow T^2$ and consequently the electrical conductivity is infinite in the non-interacting case.

These considerations give rise to a sensible Ansatz describing the high temperature vector spectral function:

$$\rho_{ii}(\omega) = 2\chi_q c_{BW} \frac{\omega \Gamma/2}{\omega^2 + (\Gamma/2)^2} + \frac{3}{2\pi} (1+k) \omega^2 \tanh(\omega/4T). \quad (7)$$

this Ansatz depends on four temperature dependent parameters; the quark number susceptibility $\chi_q(T)$, the strength ($c_{BW}(T)$) and width ($\Gamma(T)$) of the Breit-Wigner peak and the parameter $k(T)$ that parametrizes deviations from a free spectral function at large energies.

In the following we will use this Ansatz to extract the electrical conductivity and the vector spectral function from the correlator data.

2.1 Moments of the vector spectral function

In addition to the vector correlation function itself we will calculate its curvature at the largest Euclidean time separation accessible at non-zero temperature, *i.e.* at $\tau T = 1/2$. The curvature is the second thermal moment of the spectral functions at vanishing momentum,

$$G_H^{(n)} = \frac{1}{n!} \left. \frac{d^n G_H(\tau T)}{d(\tau T)^n} \right|_{\tau T=1/2} = \frac{1}{n!} \int_0^\infty \frac{d\omega}{2\pi} \left(\frac{\omega}{T}\right)^n \frac{\rho_H(\omega)}{\sinh(\omega/2T)}, \quad H = ii, V, \quad (8)$$

where n is chosen to be even as all odd moments vanish. These thermal moments give the Taylor expansion coefficients for the correlation function expanded around the mid-point of the Euclidean time interval,

$$G_H(\tau T) = \sum_{n=0}^{\infty} G_H^{(2n)} \left(\frac{1}{2} - \tau T\right)^{2n}. \quad (9)$$

In the infinite temperature, free field limit the integral in Eq. 2 can be evaluated analytically [13] and one straight forwardly obtains the first three non-vanishing moments for massless quarks

$$G_V^{(0),free} = \frac{2}{3} G_{ii}^{(0),free} = 2T^3, \quad G_H^{(2),free} = \frac{28\pi^2}{5} T^3, \quad G_H^{(4),free} = \frac{124\pi^4}{21} T^3. \quad (10)$$

Note here that all thermal moments, $G_H^{(2n)}$ with $n \geq 0$, will be sensitive to the smeared δ -function contributing to $\rho_{ii}(\omega)$ although we expect this contribution to become more and more suppressed in higher order moments [1].

In the following we will analyze the ratio of $G_H(\tau T)$ and the free field correlator $G_H^{free}(\tau T)$,

$$\frac{G_H(\tau T)}{G_H^{free}(\tau T)} = \frac{G_H^{(0)}}{G_H^{(0),free}} \left(1 + \left(R_H^{(2,0)} - R_{H,free}^{(2,0)} \right) \left(\frac{1}{2} - \tau T\right)^2 + \dots \right), \quad (11)$$

as well as the ratio of mid-point subtracted correlation functions

$$\begin{aligned} \Delta_H(\tau T) &\equiv \frac{G_H(\tau T) - G_H^{(0)}}{G_H^{free}(\tau T) - G_H^{(0),free}} \\ &= \frac{G_H^{(2)}}{G_H^{(2),free}} \left(1 + \left(R_H^{(4,2)} - R_{H,free}^{(4,2)} \right) \left(\frac{1}{2} - \tau T\right)^2 + \dots \right). \end{aligned} \quad (12)$$

Here we used the notation $R_H^{(n,m)} \equiv G_H^{(n)}/G_H^{(m)}$. Note that the curvature of these ratios at the mid-point determines the deviation of ratios of thermal moments from the corresponding free field values. While the ratios of correlation functions differ in the $H = ii$ and $H = V$ channels due to the additional constant contributing to $G_V(\tau T)$, this constant drops out in the subtracted correlation function, *i.e.*, $\Delta_V(\tau T) \equiv \Delta_{ii}(\tau T)$ and $G_V^{(n)} = G_{ii}^{(n)}$ for $n > 0$.

3 Temperature dependence of the vector spf on the lattice

The numerical results presented here are an extension to our earlier study and comprise calculations that have been performed at several temperatures $1.16T_c \lesssim T \lesssim 2.98T_c$. Consequently all parameters were chosen and adjusted following the procedures outlined in [1]. As such they are obtained from

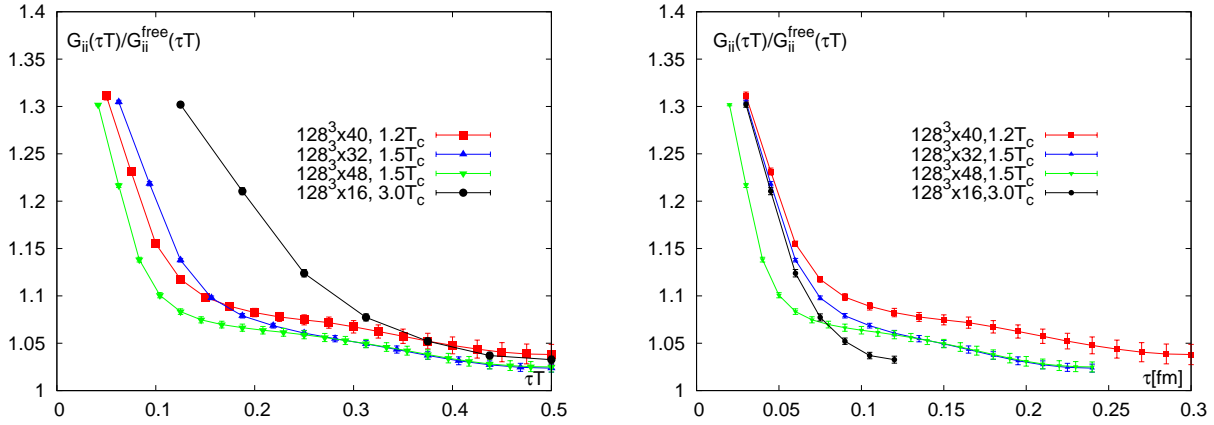


Figure 1: The vector correlation function normalized by its free continuum counterpart at varying temperature in τT (left) and [fm] (right).

quenched QCD gauge field configurations generated with the standard SU(3) single plaquette Wilson gauge action [14] using the clover improved Wilson action with non-perturbatively chosen clover coefficient c_{SW} [15] in the fermion sector. The temperature range is then varied by keeping the gauge coupling fixed for different temporal lattice sizes $N_\tau = 16, 32, 40$. Note here throughout we also show results at $T \simeq 1.45T_c$ for $N_\tau = 48$ for comparison. The simulation parameters are given in Tab. 1.

In Fig. 1 we show the ratio $G_{ii}(\tau T)/G_{ii}^{free}$ for the $\beta = 7.457$ and the $\beta = 7.793$ (green points) lattices in Euclidean temperature units (left) and in physical distance (right). On the right of Fig. 1 we see that the $\beta = 7.457$ lattices lie on top of each other for $\tau \lesssim 0.06\text{fm}$, in view of the results at $\beta = 7.793$ this can be understood as due to cut-off effects. As such the cut-off effects dominate the low distance region of the correlation function, in the presented calculations however the cut-off is fixed and therefore we expect them to be the same throughout. At $\tau \gtrsim 0.06\text{fm}$ the deviations should subsequently be due to temperature effects. Notice however that the first 6 to 8 points in the correlator are dominated by the cut-off and consequently the $N_\tau = 16$ results are more affected by the cut-off effects throughout the Euclidean time interval. Nevertheless the $N_\tau = 16$ results in Fig. 1 (left) level out in the regime $\tau T \gtrsim 0.4$. Note the correlator ratio from the $T \simeq 1.16T_c$ lattice exhibits a visibly larger value for all Euclidean times, even though its trend is similar to that at $T \simeq 1.49T_c$.

3.1 Temperature dependence of the thermal moments

Calculating the temperature dependence of the thermal moments we compute the quantity $\Delta_H(\tau T)$ and then fit to a quartic Ansatz. Using a jackknife procedure we then immediately calculate the ratio $R_{ii}^{(2,0)}/R_{ii}^{(2,0),free}$ and the corresponding results over T/T_c are shown in Fig. 2. Note here we also give the $N_\tau = 16$ and continuum extrapolated results at $T \simeq 1.45T_c$ taken from [1] for comparison. Additionally

N_τ	N_σ	# conf	β	$a[\text{fm}]$	T/T_c	c_{SW}	κ	$m_{\overline{MS}}/T_{[\mu=2\text{GeV}]}$	Z_V
40	128	451	7.457	0.015	1.16	1.3389	0.13390	0.0989(4)	0.851
32	128	255	7.457	0.015	1.49	1.3389	0.13390	0.0989(4)	0.851
16	128	340	7.457	0.015	2.98	1.3389	0.13390	0.0989(4)	0.851
48	128	191	7.793	0.010	1.45	1.3104	0.13340	0.1117(2)	0.861

Table 1: Parameters for the calculation of vector correlation functions on lattices of size $N_\sigma^3 \times N_\tau$.

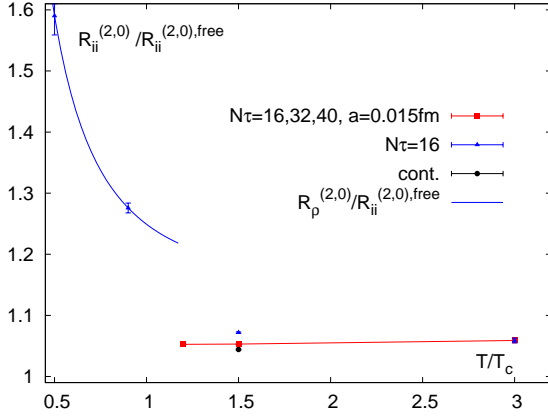


Figure 2: Left: The ratio $R_{ii}^{(2,0)}/R_{ii}^{(2,0),free}$ over T/T_c above and below T_c . Shown are the results for $\beta = 7.457$ (red) and the continuum extrapolation at $T \simeq 1.45T_c$ (black). Additionally a number of results from $N_\tau = 16$ lattices at varying temperatures (blue) are given, including also results that have been obtained using data from [16]. Right: Table of results for $R_{ii}^{(2,0)}/R_{ii}^{(2,0),free}$.

here we also show points below T_c from calculations done by the Bielefeld lattice group that have already been examined in [16].

Above T_c , i.e. in temperature region evaluated here $1.16T_c \lesssim T \lesssim 2.98T_c$, the data points are seen to be almost constant in T/T_c . Turning to the table on the right of Fig. 2 we identify a slight rise of the ratio within 0.5% going from $\simeq 1.49T_c$ and $N_\tau = 32$ to $\simeq 2.98T_c$ and $N_\tau = 16$.

Below T_c on the other hand we immediately identify a clear temperature dependence of the ratio $R_{ii}^{(2,0)}/R_{ii}^{(2,0),free}$. As such there is a 30% difference between the results at $T \simeq 0.55T_c$ and $T \simeq 0.93T_c$. At the same time the result at $T \simeq 0.93T_c$ is roughly 20% larger than that encountered above T_c .

Together the drop below and the constant behavior above T_c are very interesting from the point of view of a possible ρ -resonance in the spectrum. As such we estimate the impact of a ρ -resonance on the ratio of thermal moments $R_{ii}^{(2,0)}/R_{ii}^{(2,0),free}$ by assuming the ρ -resonance to contribute a single cosh in the correlator:

$$G_\rho(\tau) = A \cdot \cosh \left[\frac{m_\rho}{T} \cdot \tau T \right] \quad , \quad (13)$$

taking the second derivative in τT of $G_\rho(\tau)$ then gives the second thermal moment, thus we find:

$$R_\rho^{(2,0)} = \left(\frac{m_\rho}{T} \right)^2 = \left(\frac{m_\rho}{T_c} \right)^2 \cdot \left(\frac{T_c}{T} \right)^2 \quad . \quad (14)$$

As a consequence we expect the ratio $R_\rho^{(2,0)}$ to go like $\sim 1/T^2$. Adding also a continuous contribution to this model ratio we arrive at the following estimate for the temperature dependence below T_c :

$$R_{T < T_c}^{(2,0)} = c_{cont} + \left(\frac{c_\rho m_\rho}{T_c} \right)^2 \cdot \left(\frac{T_c}{T} \right)^2 \quad . \quad (15)$$

Even though we have only two points below T_c we can nevertheless fit this estimate to the data and the result is shown as blue line in Fig. 2. The qualitatively very different behavior above and below T_c , subsequently leads us to conclude that the drop of the ratio $R_{ii}^{(2,0)}/R_{ii}^{(2,0),free}$ below T_c is in fact mostly due to a particle contribution. At the same time the constant behavior of the ratio above T_c suggests that the ρ -resonance does not or only very weakly contribute in the examined temperature range.

T/T_c	$\tau_{min}T$	$2c_{BW}\tilde{\chi}_q/\tilde{\Gamma}$	$\tilde{\Gamma}$	$k/\tilde{\chi}_q$	χ^2/dof	$1/C_{em} \cdot \sigma/T$
2.98	0.396	0.93(19)	3.07(70)	0.160(19)	0.54	0.31(7)
	0.354	0.91(11)	2.93(78)	0.166(11)	0.72	0.30(4)
	0.3125	0.90(8)	3.08(36)	0.189(6)	1.37	0.30(3)
	0.25	0.71(2)	3.75(14)	0.122(4)	2.07	0.24(1)
1.49	0.396	0.98(23)	3.14(80)	0.165(23)	0.01	0.33(8)
	0.354	0.97(11)	3.16(40)	0.166(11)	0.07	0.32(4)
	0.3125	0.92(4)	3.47(16)	0.164(7)	0.26	0.31(1)
	0.25	0.90(2)	3.53(10)	0.170(4)	1.16	0.30(1)
1.16	0.396	1.00(34)	3.25(12)	0.235(38)	0.01	0.33(11)
	0.354	0.99(17)	3.30(62)	0.236(18)	0.01	0.33(6)
	0.3125	0.88(6)	3.89(20)	0.233(12)	0.05	0.29(7)
	0.25	0.87(4)	3.89(18)	0.242(6)	0.14	0.29(1)

Table 2: The fit parameters of the Breit-Wigner+continuum Ansatz for $T \simeq 2.98T_c$, $1.49T_c$ and $T \simeq 1.16T_c$ on lattices with temporal extent $N_\tau = 16, 32$ and 40 . Note the fit window is varied between $\tau_{min}T = 0.25$ and $\tau_{min}T = 0.396$. .

3.2 Consequences for the vector spectral function

To discuss the consequences of our findings on the vector spectral function we invoke the Breit-Wigner+continuum Ansatz defined in Eq.7 and fit to the $T \simeq 1.16T_c$, $1.49T_c$ and $T \simeq 2.98T_c$ data respecting also the thermal moments. Additionally we analyze the dependence of the fit parameters on $\tau_{min}T$, as, with the data being subject to potentially large lattice effects, we expect large errors originating from the fit-window we choose. The resulting parameters are summarized in Tab. 2.

Here it can be seen that the results at $\tau_{min}T = 0.396$ and $\tau_{min}T = 0.354$ have the largest errors, nevertheless these results should be closest to those in the continuum as only the furthest distance points are comparatively free of lattice effects. Without a continuum extrapolation however it is at this point not possible to cleanly discern the residual deviation due to the lattice cut-off. Decreasing $\tau_{min}T$ on the other hand leads to visible systematic trends in the parameters, as such the correction term $k/\tilde{\chi}_q = kT^2/\chi_q$ and the width $\tilde{\Gamma} = \Gamma/T$ both increase with decreasing $\tau_{min}T$, while the electrical conductivity decreases. Additionally the χ^2/dof increases with decreasing $\tau_{min}T$ implying a lower quality fit with lower $\tau_{min}T$. In light of the argument above these results show that indeed the lattice effects influence the fit more strongly with smaller $\tau_{min}T$, as they cannot be taken care of by the employed Ansatz. Consequently we attribute the largest part of the systematic trends observed above to the lattice effects.

Focusing on the parameters themselves note that the correction factor $k(T)$ is the most accurately determined. Clearly it shows an increasing trend with decreasing temperature differing by a factor ~ 1.5 between $T \simeq 2.98T_c$ and $T \simeq 1.16T_c$. However as $k(T)$ is coupled to the strong coupling via $k(T) \simeq \alpha_s/\pi$ [9], this behavior is expected. The same can be seen for the width $\tilde{\Gamma}$ and the parameter $2c_{BW}\tilde{\chi}_q/\tilde{\Gamma} = 2c_{BW}\chi_q/(\Gamma T)$, they also slightly increase with decreasing temperature. However here, they remain within errors of each other and the increase between $T \simeq 2.98T_c$ and $T \simeq 1.16T_c$ is small. Naturally this also leads to only small deviations of the electrical conductivity. Note however that the results at $N_\tau = 16$ differ by $\simeq 5\%$ from those of $N_\tau = 32$, while this deviation is only $\simeq 2\%$ for $N_\tau = 40$. With the $N_\tau = 16$ lattice being most affected by the systematics of the fit, we assume the largest part of this deviation to find its origins there. Even so we find the electrical conductivity to be to a good degree constant and within $\simeq 7\%$ across the temperature region evaluated here, whereby the values at the individual temperatures have fit errors around $\simeq (7 - 11)\%$.

In the temperature range $1.16T_c \lesssim T \lesssim 2.98T_c$ Our results therefore imply that the electrical conductivity depends linearly on temperature as expected from perturbation theory [6] and at $\beta = 7.457$ we find the value:

$$\sigma = (0.33 \pm 0.04 \pm 0.11) \cdot C_{em} \cdot T \quad , \quad (16)$$

whereby the first error quoted corresponds to the temperature effects and the second to the fit errors.

4 Conclusions

Extending our earlier study we presented results on the vector correlation function in the high temperature phase of quenched QCD in the temperature range $1.16T_c \lesssim T \lesssim 2.98T_c$. First results show a similar behavior to those extensively analyzed at $T \simeq 1.45T_c$ and even at $T \simeq 1.16T_c$ we find no sizable contribution attributable to the ρ -resonance.

Even though these calculations could not yet be extended to include also a continuum extrapolation as in [1], we were nevertheless able to extract the relevant spectral properties to calculate the electrical conductivity via an Ansatz and found this phenomenologically relevant transport coefficient to depend linearly on temperature with a value of $\sigma = (0.33 \pm 0.04 \pm 0.11) \cdot C_{em} \cdot T$.

Given the exact relation between the electrical conductivity and the diffusion constant, $\sigma = \chi_q D$, it would be interesting to compare these results with those obtained in the case of charm diffusion [17] or from the momentum diffusion constant κ calculable via HQET [18, 19] and we will do so in an upcoming publication.

References

- [1] H. T. Ding., A. Francis, O. Kaczmarek, F. Karsch, E. Laermann and W. Söldner, *Phys. Rev. D* 83 (2011) 034504 ; O. Kaczmarek, A. Francis, *J.Phys.G* G38 (2011) 124178
- [2] for an overview and further references, see for instance: F. Gelis, *Nucl. Phys. A* 715 (2003) 329
- [3] J. P. Blaizot and F. Gelis, *Eur. Phys. J. C* 43 (2005) 375
- [4] E. Braaten and R.D. Pisarski, *Nucl. Phys. B* 337 (1990) 569
- [5] F. Karsch, M. G. Mustafa and M. H. Thoma, *Phys. Lett. B* 497 (2001) 249
- [6] P. B. Arnold, G. D. Moore and L. G. Yaffe, *JHEP* 0011 (2000) 001 ; *JHEP* 0112 (2001) 009 ; *JHEP* 0305 (2003) 051
- [7] P. Aurenche, F. Gelis, G. D. Moore and H. Zaraket, *JHEP* 0212 (2002) 006
- [8] S. Gupta, *Phys. Lett. B* 597 (2004) 57 ; G. Aarts et al., *Phys. Rev. Lett.* 99 (2007) 022002
- [9] T. Altherr and P. Aurenche, *Z. Phys. C* 45 (1989) 99
- [10] G. Aarts and J. M. Martinez Resco, *JHEP* 0204 (2002) 053
- [11] P. Petreczky and D. Teaney, *Phys. Rev. D* 73 (2006) 014508
- [12] J. Hong and D. Teaney, *Phys. Rev. C* 82 (2010) 044908
- [13] W. Florkowski and B.L. Friman, *Z. Phys. A* 347 (1994) 271
- [14] K. G. Wilson, *Phys. Rev. D* 10 (1974) 2445
- [15] M. Lüscher, S. Sint, R. Sommer, P. Weisz and U. Wolff, *Nucl. Phys. B* 491 (1997) 323
- [16] S. Wissel, PhD-Thesis Bielefeld University (2006)
- [17] H. T. Ding, A. Francis, O. Kaczmarek, F. Karsch, H. Satz and W. Söldner, hep-lat/1107.0311
- [18] A. Francis, O. Kaczmarek, M. Laine, J. Langelage, hep-lat/1109.3941
- [19] D. Banerjee, S. Datta, R. Gavai, P. Majumdar, hep-lat/1109.5738